On Indoor Localization Using Magnetic Field-Aided Inertial Navigation Systems

Chuan Huang

Main Supervisor: Assoc. Prof. Isaac Skog (KTH)

Co-supervisor: Assoc. Prof. Gustaf Hendeby

Licentiate Seminar **2024.09**

LINKÖPING UNIVERSITY

Background

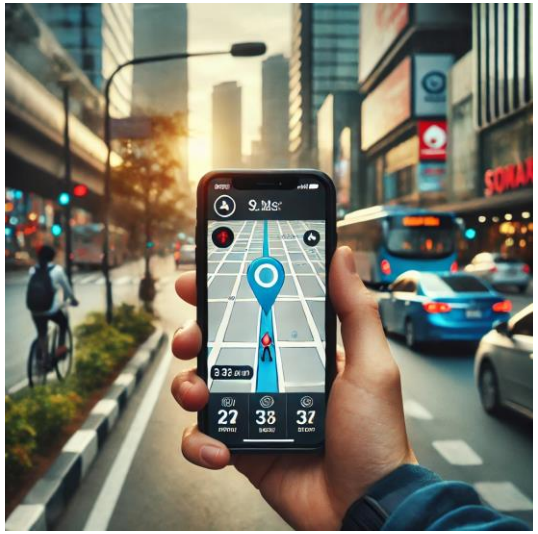


Localization and navigation technologies are vital components of modern society.

Challenges

Russia blamed for GPS interference affecting flights in Europe

2 May 2024

Vitaly Shevchenko
Russia editor, BBC Monitoring

Could the world cope if GPS stopped working?

6 November 2019

Tim Harford
Presenter, 50 Things That Made the Modern Economy

ACE AEROSPACE CENTRAL EUROPE

NAVIGATING THE ATLANTIC: FIRST-EVER GPS JAMMING ON COMMERCIAL FLIGHTS

Date 20.6.2024

Will GPS spoofing slow autonomous driving?

Manuel del Castillo explains recent consumer views related to spoofing attacks and why they cause a significant threat for automakers

November 10, 2023

GPS spoofing: what's the risk for ship navigation?

GPS spoofing – or GNSS spoofing more accurately – is a much-discussed cyber-threat to ship navigation systems. With the potential for paralysed shipping lanes, collisions and even untraceable piracy incidents, what is the current state of play between the shipping industry's cyber-defences and the malicious actors who aim to cause chaos through GPS spoofing?

Chris Lo | April 15, 2019

Consortium receives UK funding for GNSS-denied tech program

September 6, 2022 - By Tracy Cozzens

Inhomogeneous magnetic field

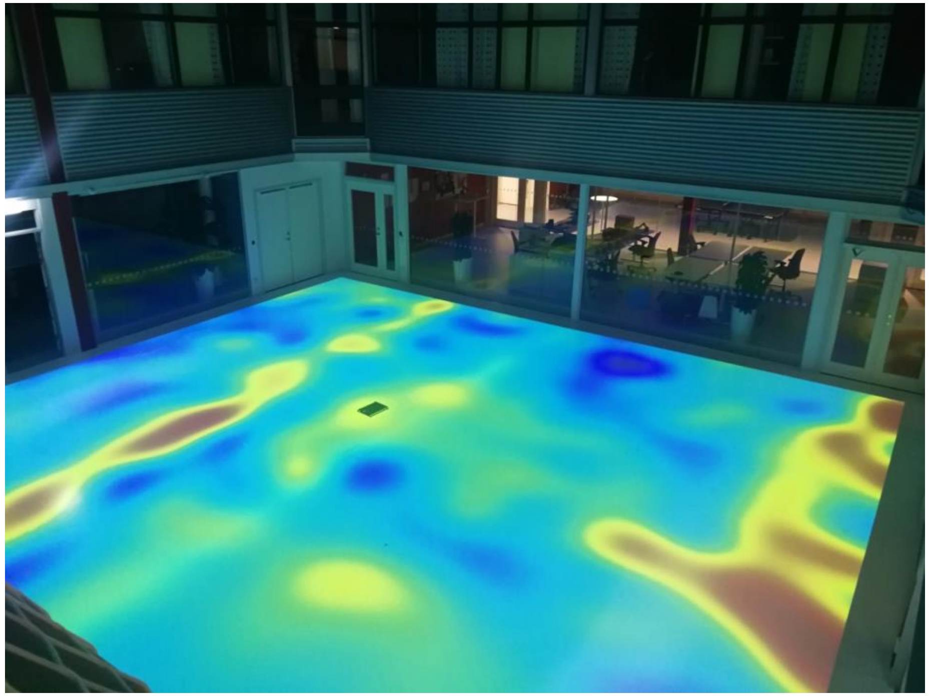

The magnetic field magnitude measured near the floor in Visionen

- Spatially varying 3D vector field
- Relatively stable (static)
- Fulfilling Maxwell's equations.

Magnetic field modeling

Global modeling

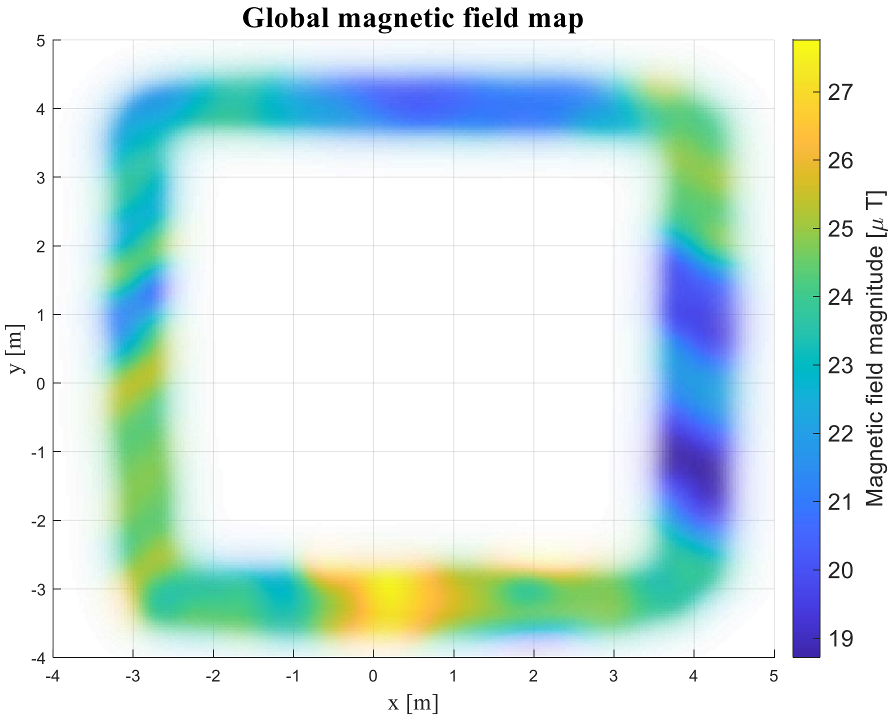

Local modeling

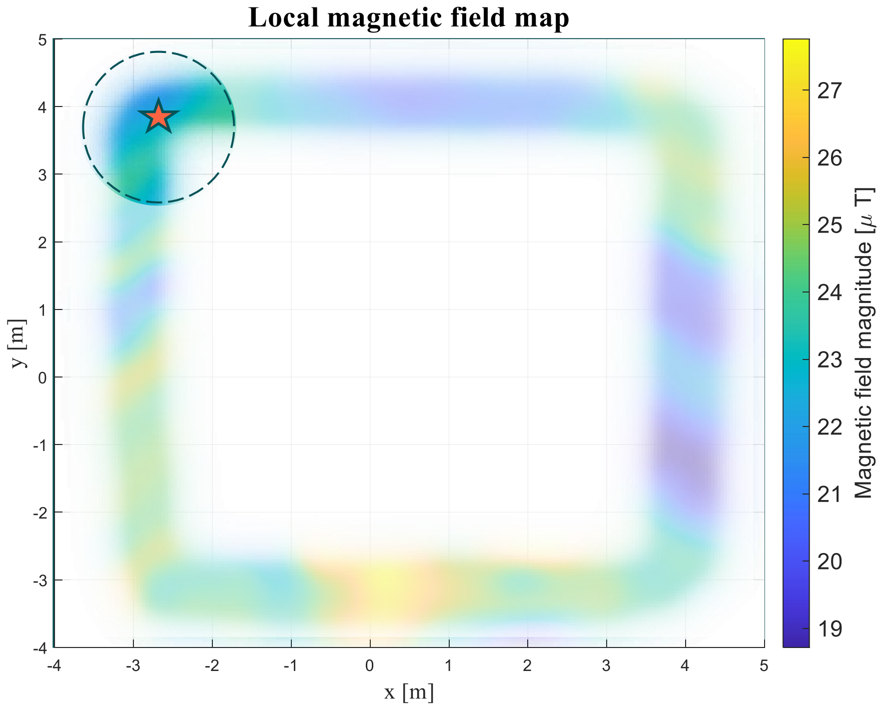

Motivation

Image #1 Image #2

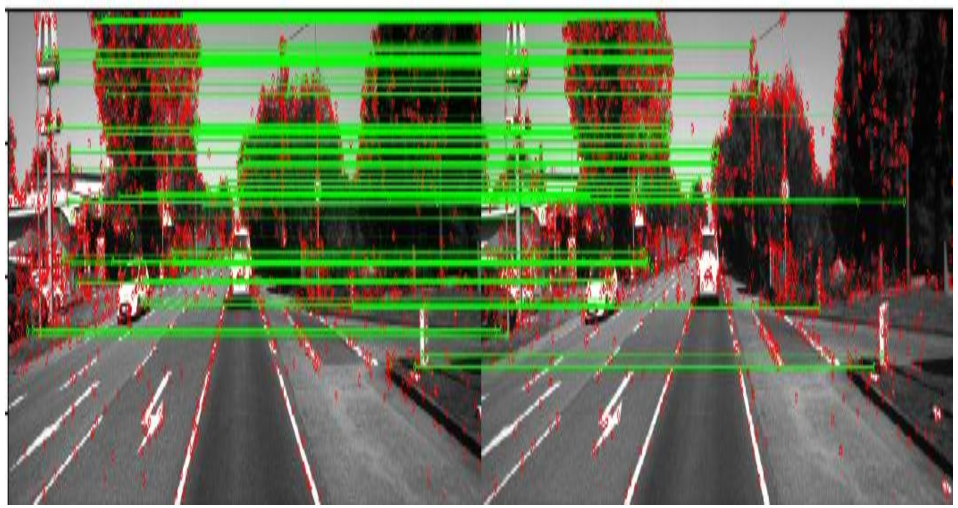

Visual images

Snapshot #1

Snapshot #2

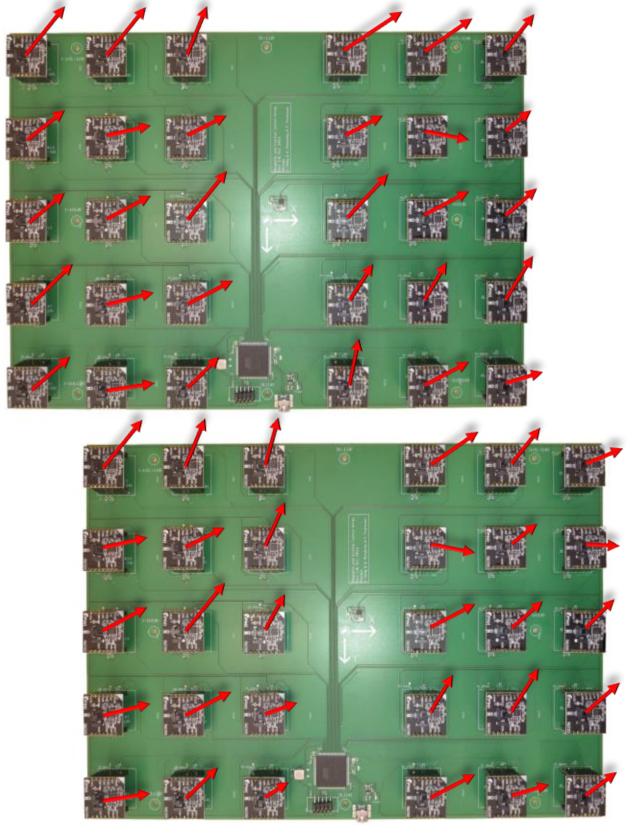

Magnetic-field images

Basic Idea

Example: 1D navigation

- 3 magnetometers
- Inertial navigation system

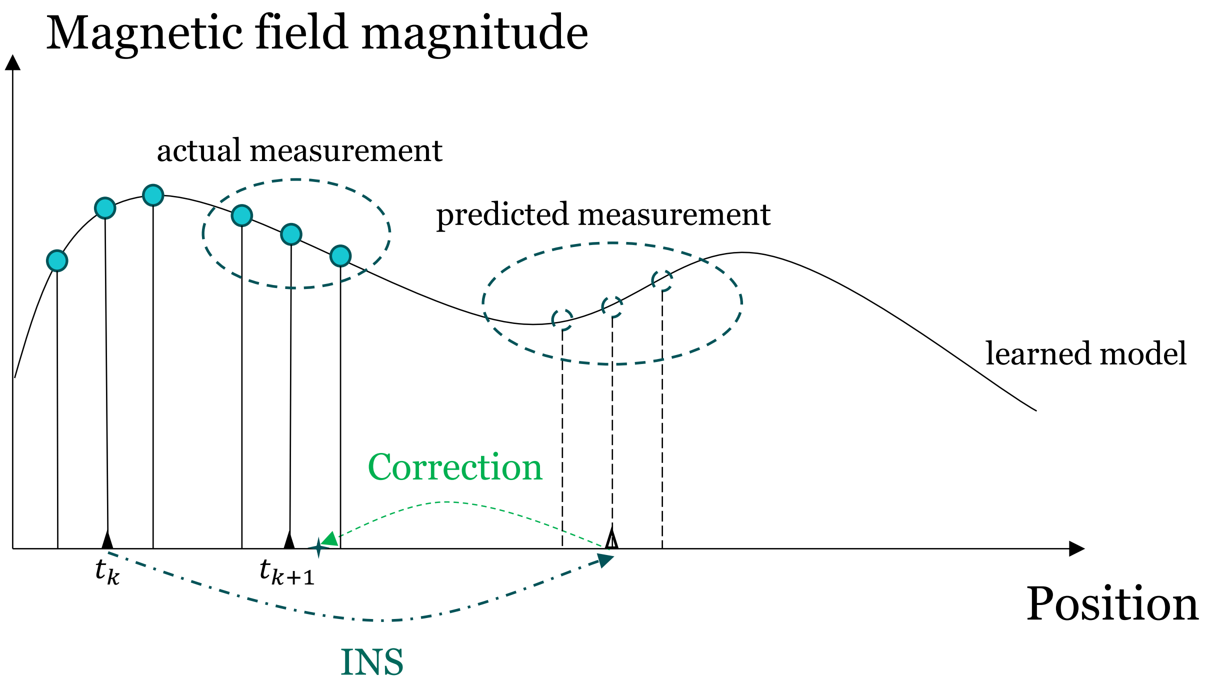

Significance

- The magnetic field-aided inertial navigation system allows indoor localization and navigation using low-cost sensors.
- It could extend the exploration phase of SLAM (simultaneous localization and mapping) systems.
- It could be incorporated into the existing magnetic field SLAM systems to boost the SLAM systems' usability.
- It could have other interesting applications: underwater navigation, medical robots, etc.

PART I
Magneto-Inertial Sensor Calibration

Common Sensor Errors

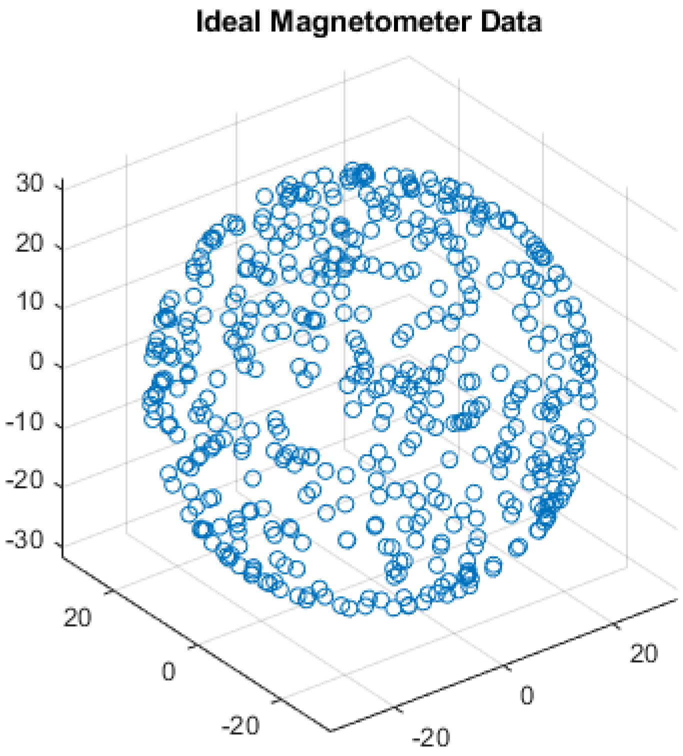

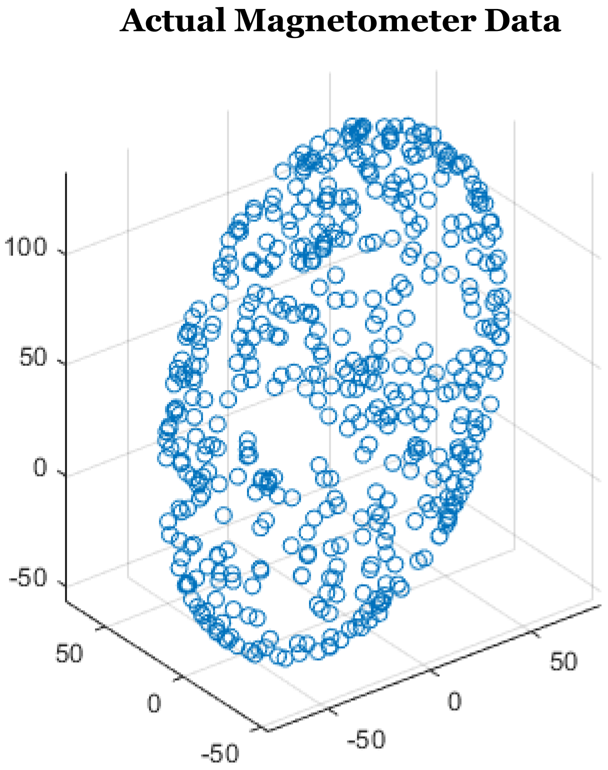

Sensor bias
Scale factors
Non-orthogonal sensitivity axes
Random noise
Frame Misalignment ……

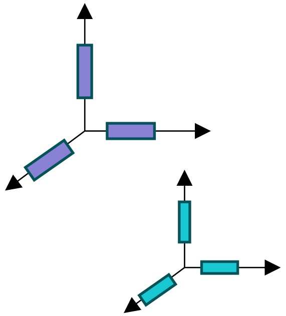

Magneto-Inertial Sensor Model

$$y_k \doteq \begin{bmatrix}\tilde{s}_k \\ \tilde{\omega}_k \\ \tilde{m}_k\end{bmatrix} = \tilde{h}(x_k, u_k; \theta) + e_k,$$

$$\tilde{h}(x_k, u_k; \theta) = \begin{bmatrix} -R_k^\top \mathrm{g}^{\mathrm{n}} + o^a \\ \omega_k + o^\omega \\ D^m R_k^\top m(\alpha) + o^m \end{bmatrix},$$

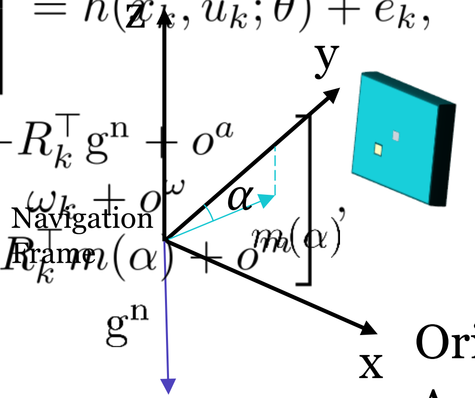

$x_k = R_k,$ Orientation matrix

$u_k = \omega_k,$ Angular velocity

$\theta = \{o^a, o^\omega, o^m, D^m, \alpha\}.$ Calibration parameters

Problem: Given $\{y_0, y_1, \cdots, y_{N-1}\}$, estimate θ.

LINKÖPING UNIVERSITY

Nonlinear Least Square Problem

$$\{\theta^*, R^*_{0:N-1}\} = \underset{\theta, R_{0:N-1}}{\arg\min}\, V(\theta, R_{0:N-1}),$$

$$V(\theta, R_{0:N-1}) = \underbrace{\frac{1}{2}\sum_{0}^{N-1} \|\tilde{s}_k + R_k^\top \mathrm{g}^{\mathrm{n}} - o^a\|^2_{\Sigma_a}}_{\text{acc. residual}} + \underbrace{\frac{1}{2}\sum_{0}^{N-1} \|\tilde{m}_k - D^m R_k^\top m(\alpha) - o^m\|^2_{\Sigma_m}}_{\text{mag. residual}}$$

$$+ \underbrace{\frac{1}{2}\sum_{0}^{N-2} \|\tilde{\omega}_k - \frac{1}{\Delta T}\mathrm{Log}_R(R_k^\top R_{k+1}) - o^\omega\|^2_{\Sigma_\omega}}_{\text{gyro. residual}}.$$

noise covariance Σ_a: accelerometer, Σ_m: magnetometer, Σ_ω: gyroscope.

ΔT: sampling interval.

$\mathrm{Log}_R : \mathrm{SO}(3) \to \mathbb{R}^3$

Practical Aspect

Calibration Requirements:

1. The sensor board must be rotated slowly to minimize acceleration.
2. The sensor system needs exposure to a wide range of orientations.

Data Collection:

- Duration: Approx. 5 minutes
- Sampling rate: 100 Hz
- Total samples: 30,000

Challenges:

- Computationally heavy: Handling large datasets requires significant processing power.
- Memory intensive: Large Jacobian matrices need extensive memory for storage.

Reason: The dimension of $R_{0:N-1}$ grows linearly with time.

Solution: Downsampling

Motivation

- $R_{0:N-1}$ are slowly varying due to slow motion/rotation.

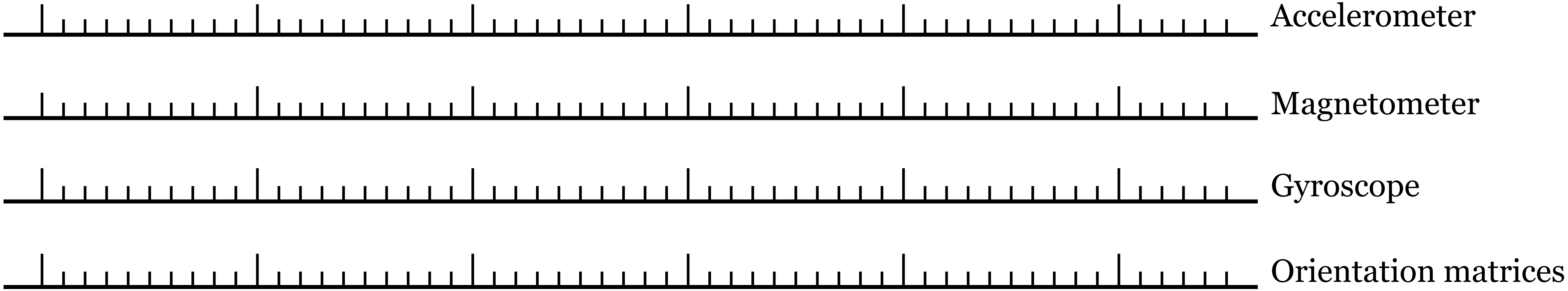

Downsample rate: $10\times$

Constructing New Residuals

$\tilde{s}_k + R_k^\top \mathrm{g}^{\mathrm{n}} - o^a$

acc. residual

$\tilde{m}_k - D^m R_k^\top m(\alpha) - o^m$

mag. residual

$\tilde{\omega}_k - \frac{1}{\Delta T}\mathrm{Log}_R(R_k^\top R_{k+1}) - o^\omega$

gyro. residual

Downsample rate: 10 ×

Gyroscope Pre-integration & Residual

Given gyroscope measurements on time interval $[t_i, t_j)$, the gyroscope pre-integration gives a probabilistic description of the orientation change, i.e.,

$$\Delta\tilde{R}_{ij} = \Delta R_{ij}\mathrm{Exp}_R(\delta\phi_{ij}).$$

$\Delta\tilde{R}_{ij} = \prod_{k=i}^{j-1} \mathrm{Exp}_R\left((\tilde{\omega}_k - o^{\omega})\Delta T\right)$ $\qquad$ $\Delta R_{ij} \doteq R_i^\top R_j$ $\qquad$ $\delta\phi_{ij} \in \mathbb{R}^3$: pre-integration noise

$$\mathrm{Exp}_R : \mathbb{R}^3 \to \mathrm{SO}(3)$$

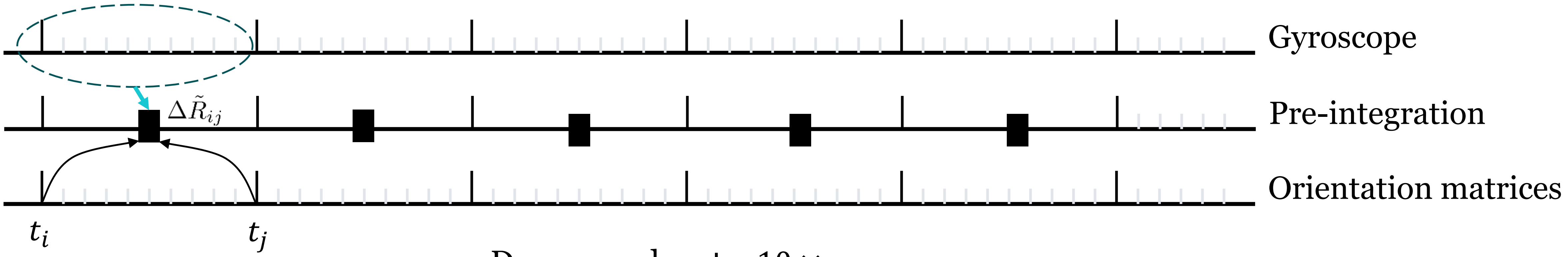

Downsample rate: 10 ×

Gyroscope Pre-integration & Residual

Given gyroscope measurements on time interval $[t_i, t_j)$, the gyroscope pre-integration gives a probabilistic description of the orientation change, i.e.,

$$\Delta\tilde{R}_{ij} = \Delta R_{ij} \mathrm{Exp}_R(\delta\phi_{ij}).$$

$$\Delta\tilde{R}_{ij} = \prod_{k=i}^{j-1} \mathrm{Exp}_R\left((\tilde{\omega}_k - o^\omega)\Delta T\right) \qquad \Delta R_{ij} \doteq R_i^\top R_j \qquad \delta\phi_{ij} \in \mathbb{R}^3\text{: pre-integration noise}$$

$$\mathrm{Exp}_R : \mathbb{R}^3 \to \mathrm{SO}(3)$$

Weighted Residual Norm Squared:

$$\|\mathrm{Log}_R(\Delta\tilde{R}_{ij} R_i^\top R_j)\|^2_{\Sigma_{ij}}, \text{ where } \Sigma_{ij} = \mathrm{Cov}(\delta\phi_{ij}).$$

Experiment Results

Real-World Experiment Setup

- Sampling rate: 500 Hz
- # of data points: 120k
- 30 magnetometers and one IMU
- Calibrate magnetometer-IMU pair one at a time
- Equivalent sampling rate: 5 Hz

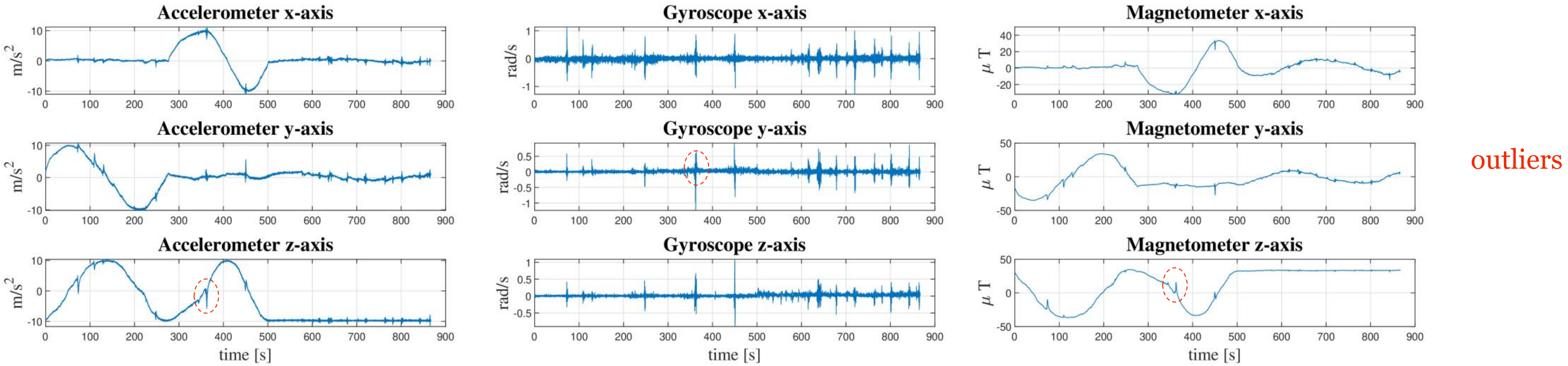

Magnetometer Calibration Result

The norm of 30 magnetometers' measurements before and after calibration

Before calibration

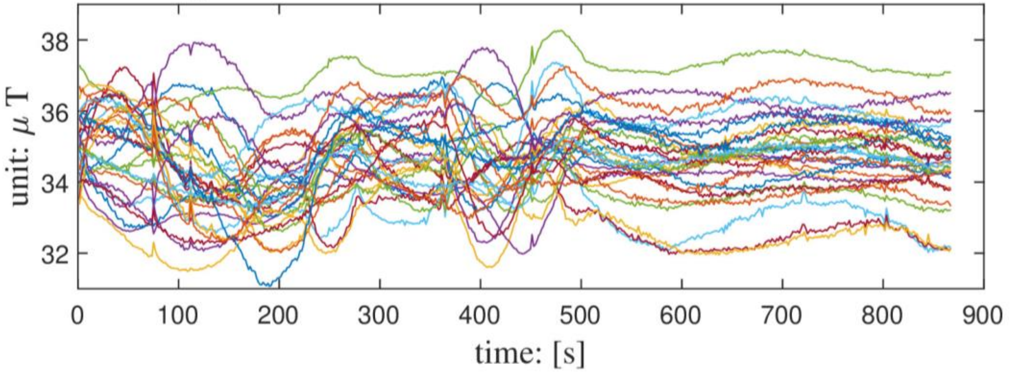

After calibration

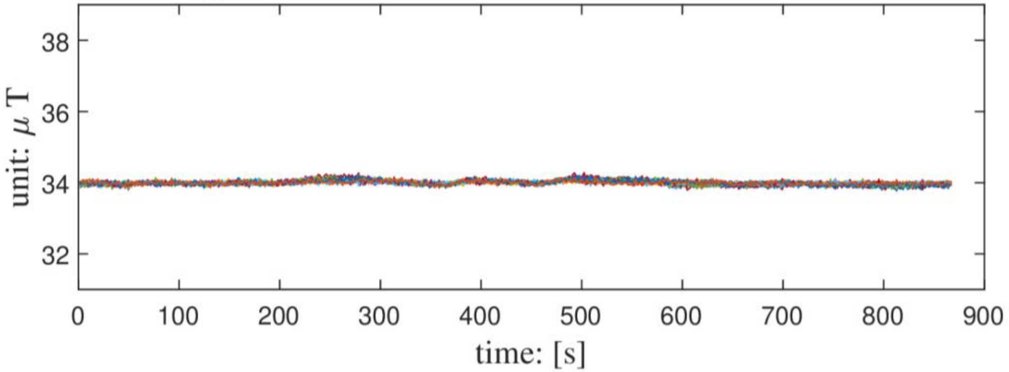

Noise standard deviation 0.015μT

- Calibration significantly reduces the variance across all magnetometers.

Conclusion

- The proposed method can significantly minimize the discrepancies

in magnetic field measurements from the sensor array.

- It is computationally efficient and saves memory.

PART Ⅱ
Magnetic Field-based Localization

The Magnetic Field-Aided Inertial Navigation System (MAINS)

MAINS: A magnetic-field-aided inertial navigation system for indoor positioning.
Chuan Huang, Gustaf Hendeby, Hassen Fourati, Christophe Prieur, and Isaac Skog.
IEEE Sensors Journal, 24(9):15156–15166, 2024.

A tightly-integrated magnetic-field aided inertial navigation system.
Chuan Huang, Gustaf Hendeby, and Isaac Skog.
In Proc. 2022 25th Int. Conf. on Information Fusion (FUSION), pages 1–8,
Linköping, Sweden, July 2022.

LINKÖPING UNIVERSITY

Overview

- Self-contained localization solution
- Positioning with Inhomogeneous magnetic fields
- Magneto-Inertial sensor array
- A tightly-integrated magnetic field odometry-aided inertial navigation system

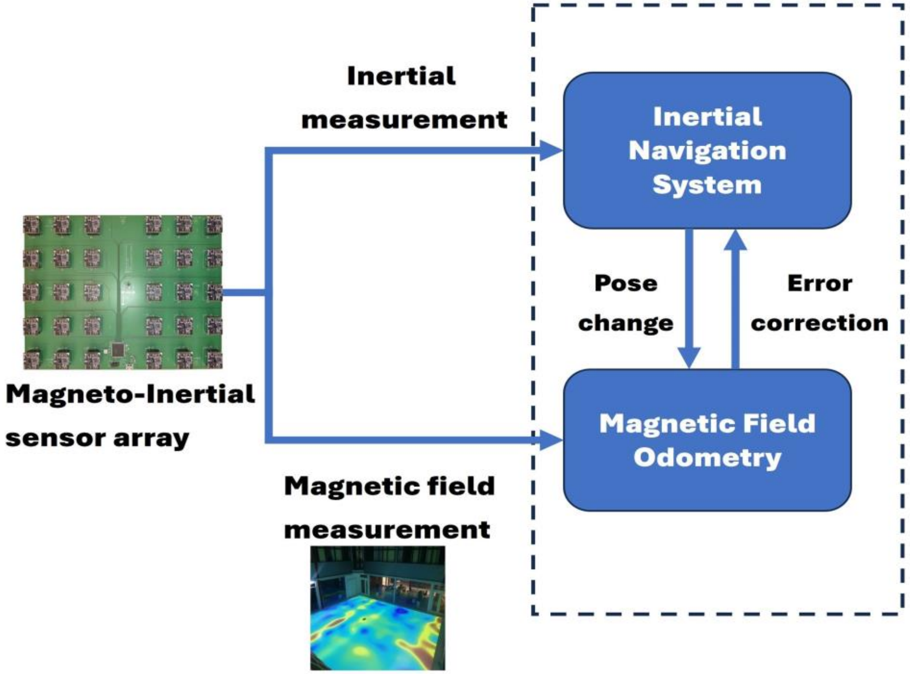

Magnetic Field Model

$M(r)$: the magnetic field vector at location r.

When there is no free current in the space and the electric field is static,

Divergence-free	$\nabla \cdot M(r) = 0,$	(1a)
Curl-free	$\nabla \times M(r) = 0.$	(1b)

Equation (1b) allows $M(r)$ to be the **gradient** of a scalar **potential function** $\phi(r)$, i.e.,

$$M(r) = \nabla_r \phi(r).$$

In this work, the scalar potential function $\phi(r)$ is chosen to be a **polynomial function**. Hence, $M(r)$ is referred to as the **polynomial magnetic field model**.

Magnetic Field Model

$$M(r;\theta) = \Phi(r)\theta.$$

$\Phi(\cdot)$: $3 \times \kappa$ matrix $\quad$ θ: $\kappa \times 1$ vector

- The magnetic field is expressed in the body frame.
- The origin of the model is aligned with the origin of the body frame.
- The location r is expressed in the body frame.
- $\Phi(r)$ is a fixed matrix for any given magnetometer's location.
- When the body frame moves, θ changes along with it.

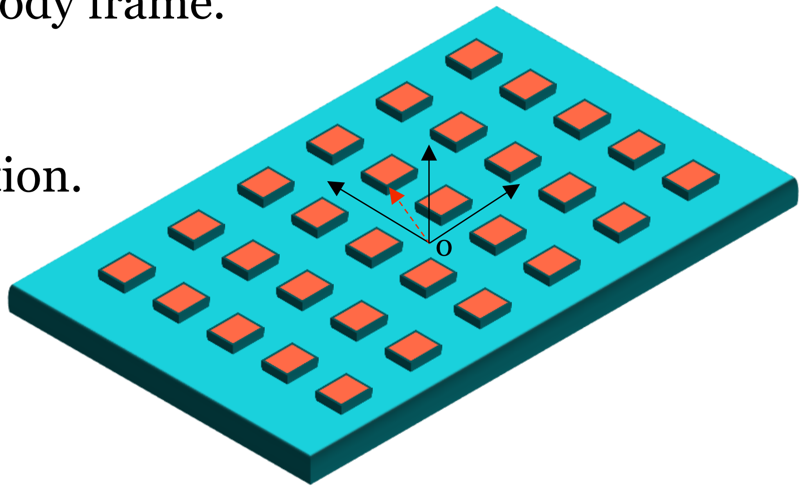

Magnetic Field Model

$$M(r;\theta) = \Phi(r)\theta.$$

- 1st order model (8 dimensional)

$$\Phi(r) = \begin{bmatrix} 0 & 0 & 1 & 0 & 0 & r_z & r_y & 2r_x \\ 0 & 1 & 0 & r_z & 2r_y & 0 & r_x & 0 \\ 1 & 0 & 0 & r_y & -2r_z & r_x & 0 & -2r_z \end{bmatrix}.$$

- 2nd order model (15 dimensional)

$$\Phi(r) = \begin{bmatrix} 0 & 0 & 1 & 0 & 0 & r_z & r_y & 2r_x & 0 & 0 & r_yr_z & r_y^2 - r_z^2 & 2r_xr_z & 2r_xr_y & 3r_x^2 - 3r_z^2 \\ 0 & 1 & 0 & r_z & 2r_y & 0 & r_x & 0 & 2r_yr_z & 3r_y^2 - 3r_z^2 & r_xr_z & 2r_xr_y & 0 & r_x^2 - r_z^2 & 0 \\ 1 & 0 & 0 & r_y & -2r_z & r_x & 0 & -2r_z & r_y^2 - r_z^2 & -6r_yr_z & r_xr_y & -2r_xr_z & r_x^2 - r_z^2 & -2r_yr_z & -6r_xr_z \end{bmatrix}.$$

State-Space Model

$$x_{k+1} = f(x_k, \tilde{u}_k, w_k) \quad (1)$$
$$y_k = Hx_k + e_k \quad (2)$$

$$f(x_k, \tilde{u}_k, w_k) = \begin{bmatrix} p_k + v_k \Delta T + s_k^n \frac{\Delta T^2}{2} \\ v_k + s_k^n T_s \\ q_k \otimes \mathrm{Exp}_q(\Delta \phi_k) \\ b_k^{(s)} + w_k^{b^{(s)}} \\ b_k^{(\omega)} + w_k^{b^{(\omega)}} \\ T(\theta_k, \psi_k) + w_k^{\theta} \end{bmatrix}, H = \begin{bmatrix} \mathbf{0} & \Phi(r^{(1)}) \\ \vdots & \vdots \\ \mathbf{0} & \Phi(r^{(N)}) \end{bmatrix}$$

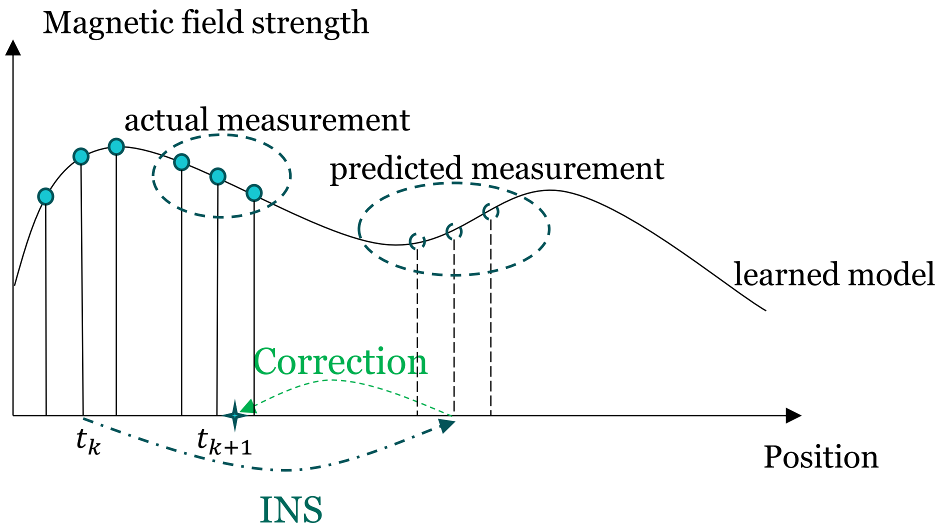

- Navigation equation
- Sensor bias random walk model
- Coefficient propagation model

$r^{(i)}$: the i^{th} magnetometer's position (in the body frame)

Experiment Results

Real-World Experiment Setup

- In total 8 datasets were collected.
- Length: 137 ~ 194 m.
- Duration: 151 s ~ 332 s.

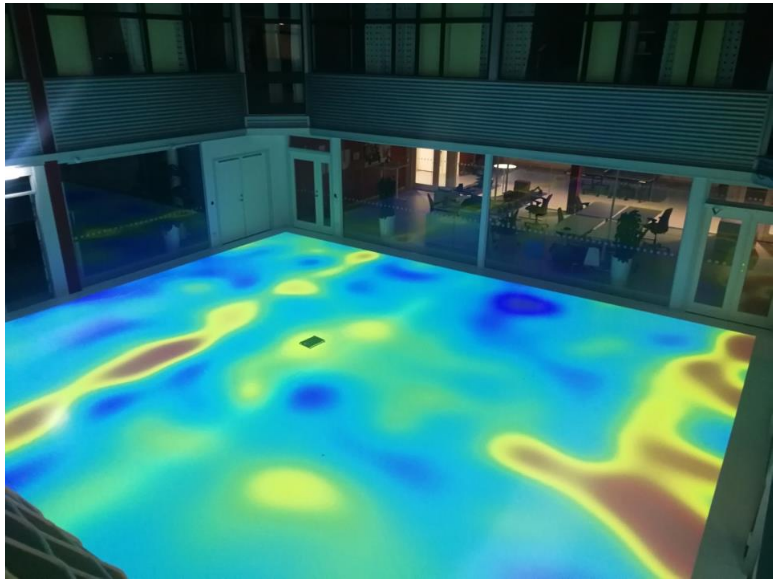

Table 4.2: Information about the datasets

Data	Length* (m)	Duration* (s)	Avg. height (m)	Board orientation
LP-1	138.72	272	0.49	parallel
LP-2	167.07	286	0.52	parallel
LP-3	194.41	332	0.55	parallel
NP-1	136.23	177	0.85	parallel
NP-2	134.66	165	0.84	parallel
NP-3	137.76	154	0.79	parallel
NT-1	164.62	185	0.73	tilted
NT-2	137.87	151	0.74	tilted

* Including the initial part of the trajectory where the position-aiding is turned on.
LP: low height and parallel NP: normal height and parallel NT: normal height and tilted.

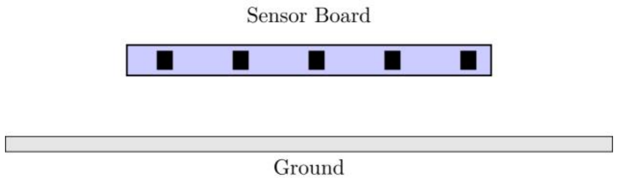

parallel

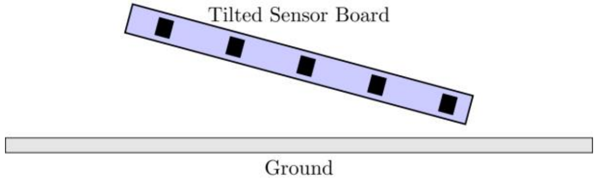

tilted

Real-World Experiment Setup

- Three algorithms: a stand-alone INS, MAINS, and the magnetic field odometry[1] .
- Position aiding for the first 60 seconds.
- For MAINS, 1st order polynomial magnetic model was used with different sensor configurations.

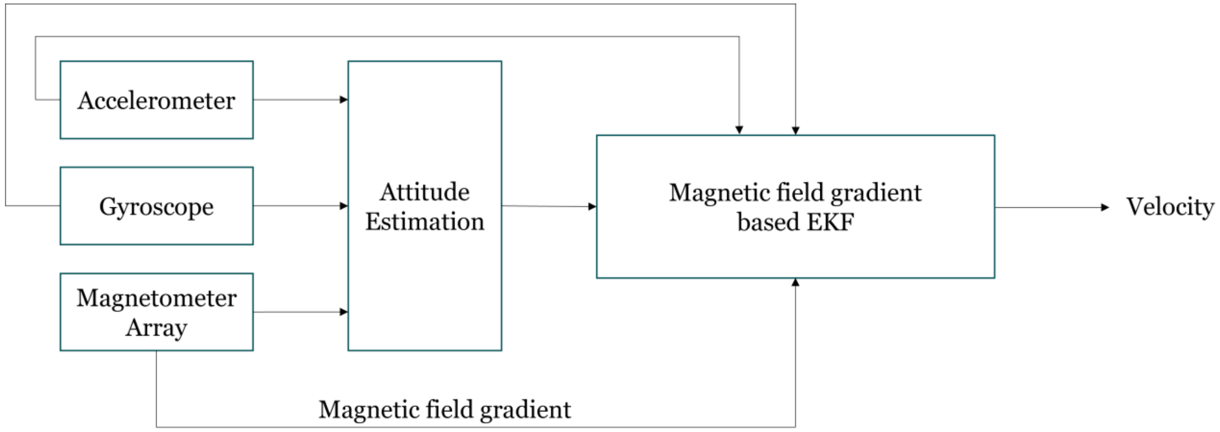

The magnetic field odometry proposed in [1]

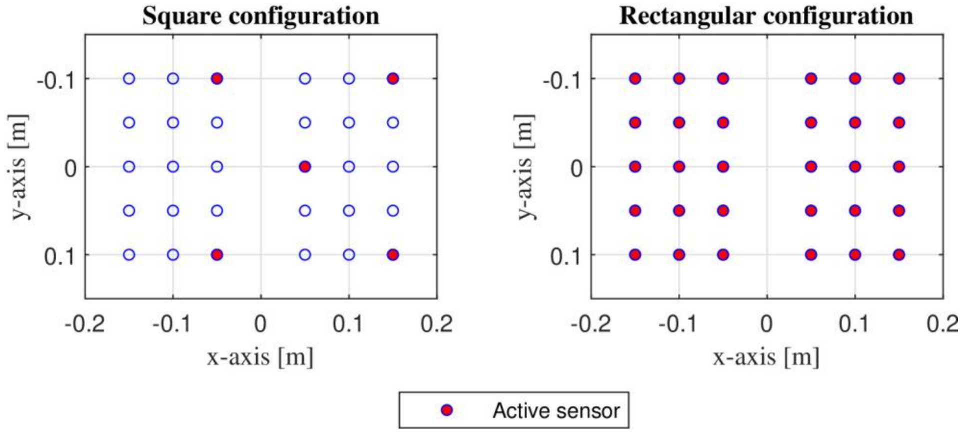

Sensor configurations

[1] Zmitri, Makia, Hassen Fourati, and Christophe Prieur. "Magnetic field gradient-based EKF for velocity estimation in indoor navigation." *Sensors* 20, no. 20 (2020): 5726.

Real-World Experiment Results

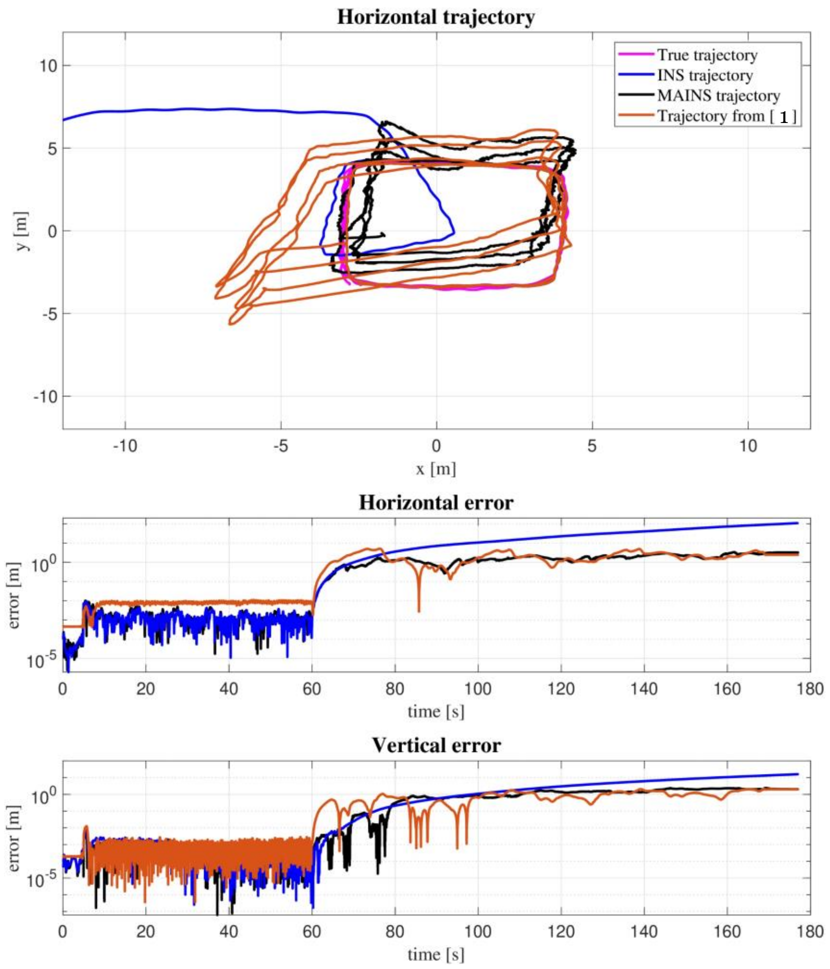

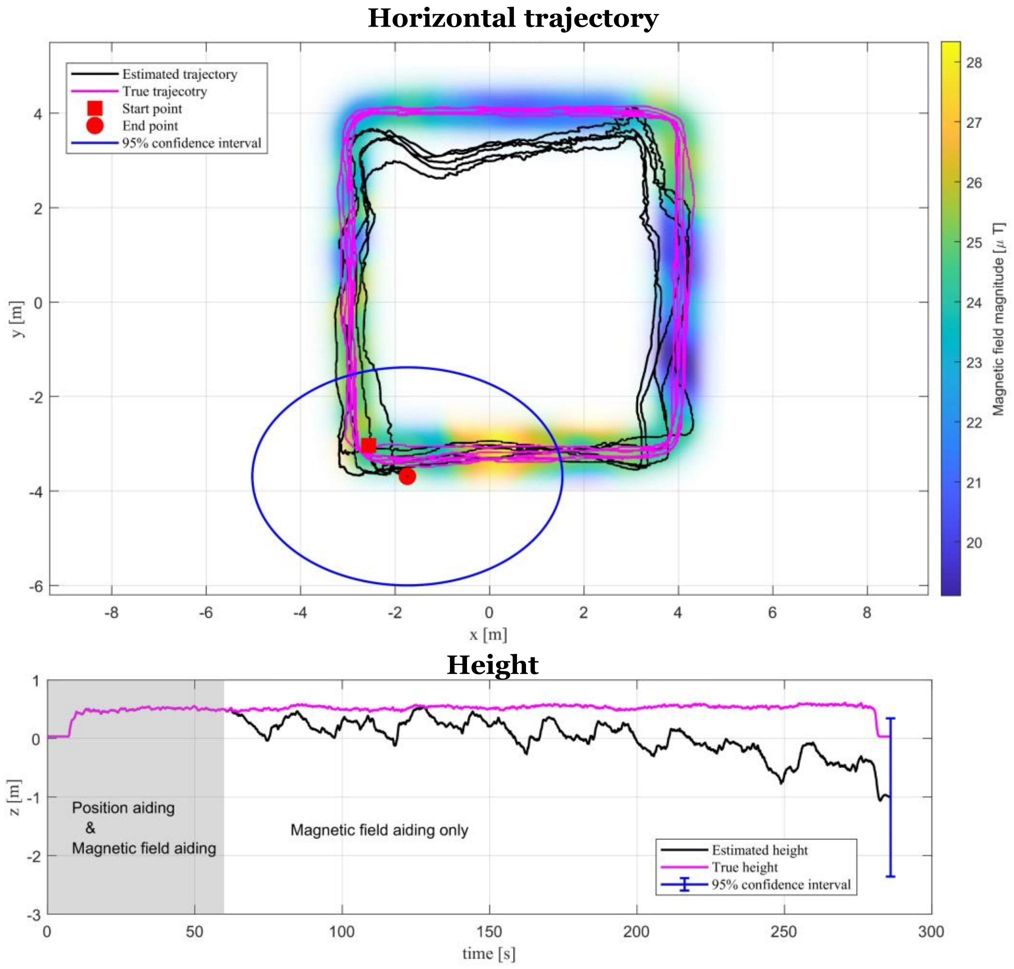

[1] Zmitri, Makia, Hassen Fourati, and Christophe Prieur. "Magnetic field gradient-based EKF for velocity estimation in indoor navigation." *Sensors* 20, no. 20 (2020): 5726.

Real-World Experiment Results

Root Mean Square (RMS) **Horizontal** Error

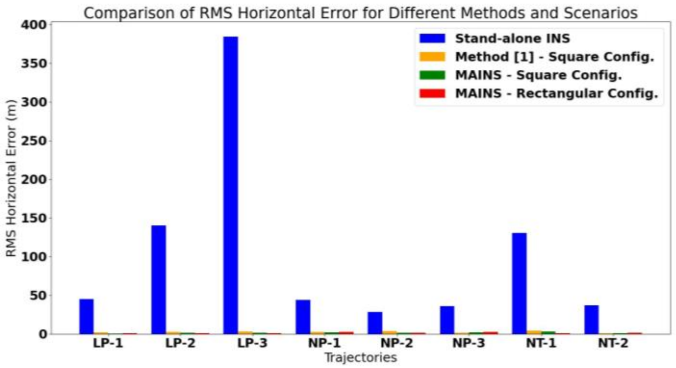

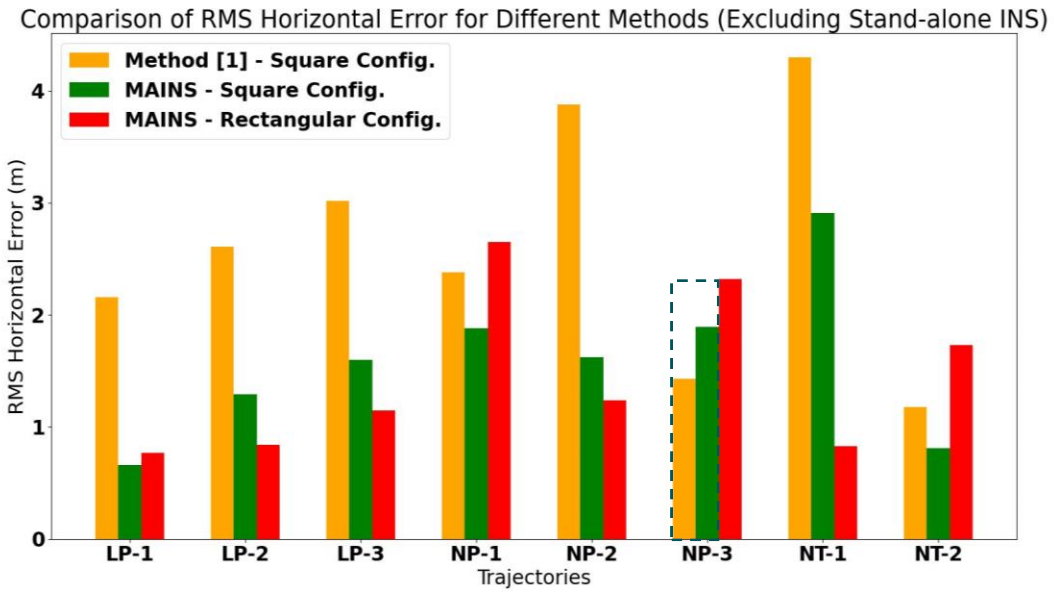

- Method [1] and MAINS outperform the stand-alone INS significantly.
- With square configuration, MAINS has lower RMS error than method [1] (expect on NP-3).
- Increasing sensors used in MAINS **does not** necessarily lead to smaller horizontal RMS error.

[1] Zmitri, Makia, Hassen Fourati, and Christophe Prieur. "Magnetic field gradient-based EKF for velocity estimation in indoor navigation." *Sensors* 20, no. 20 (2020): 5726.

Real-World Experiment Results

Root Mean Square (RMS) **Vertical** Error

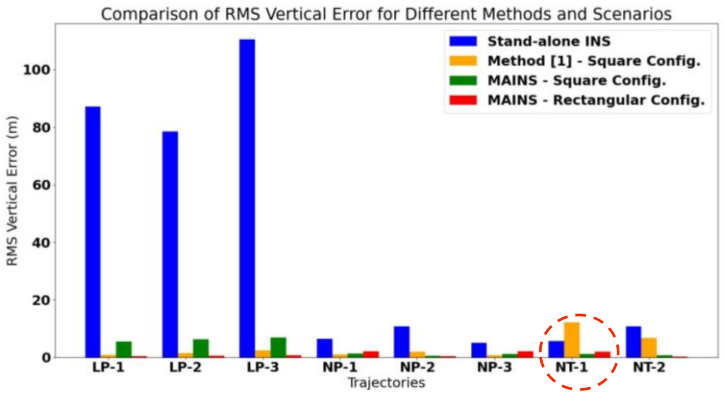

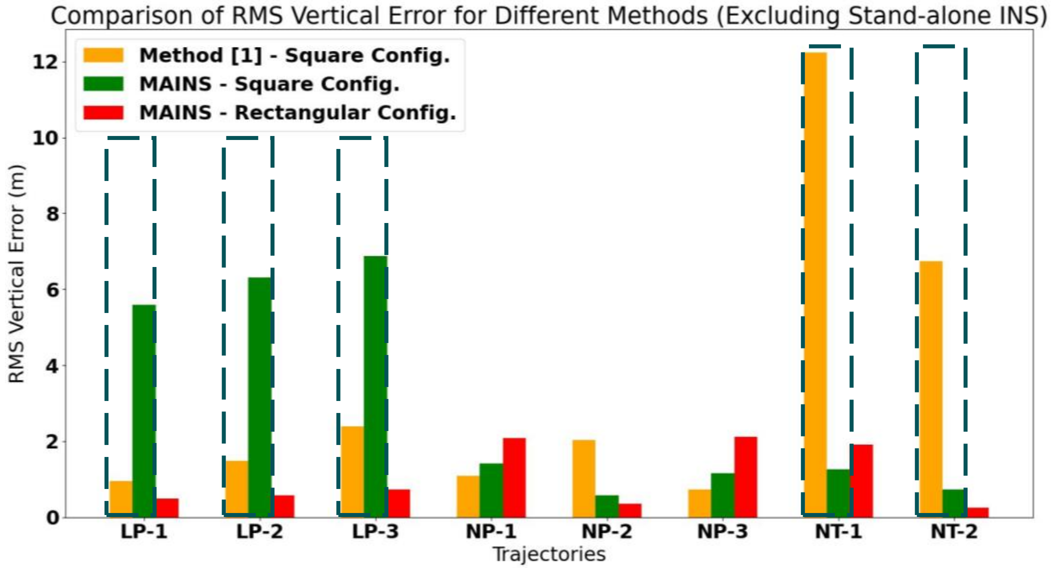

- Method [1] and MAINS outperform the stand-alone INS significantly (except on NT-1).
- With square configuration, MAINS performs **worse** than the method [1] on datasets recorded at **low altitude** but **better** on datasets where the sensor board is **tilted**.
- Increasing sensors used in MAINS **does** lead to smaller vertical RMS error when operating at **low altitude**.

[1] Zmitri, Makia, Hassen Fourati, and Christophe Prieur. "Magnetic field gradient-based EKF for velocity estimation in indoor navigation." *Sensors* 20, no. 20 (2020): 5726.

Conclusion

- A magnetic field-based indoor localization solution.
- Position drift reduction in INS significantly by 2 orders of magnitude.
- Good performance with flexible sensor configurations.
- Great possibility to be incorporated into magnetic field SLAM systems.

The Observability-Constrained Magnetic Field-Aided Inertial Navigation System (OC-MAINS)

An observability-constrained magnetic field-aided inertial navigation system.
Chuan Huang, Gustaf Hendeby, and Isaac Skog.
arXiv preprint arXiv:2406.02161. (Accepted to IPIN 2024)

LINKÖPING UNIVERSITY

Expected Behaviors

- Initially, the magnetic model have its center (origin) defined at some position.
- After correction, a new model is created, centered at the position estimate.
- The uncertainty in position will grow with time.
- The uncertainty in heading (yaw) should also grow when it comes to 3D localization.

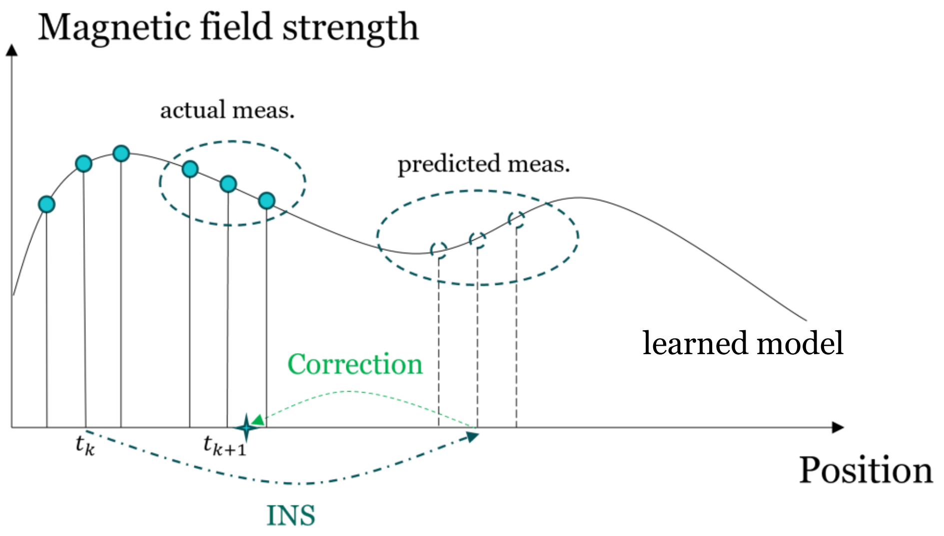

Inconsistent Yaw Uncertainty

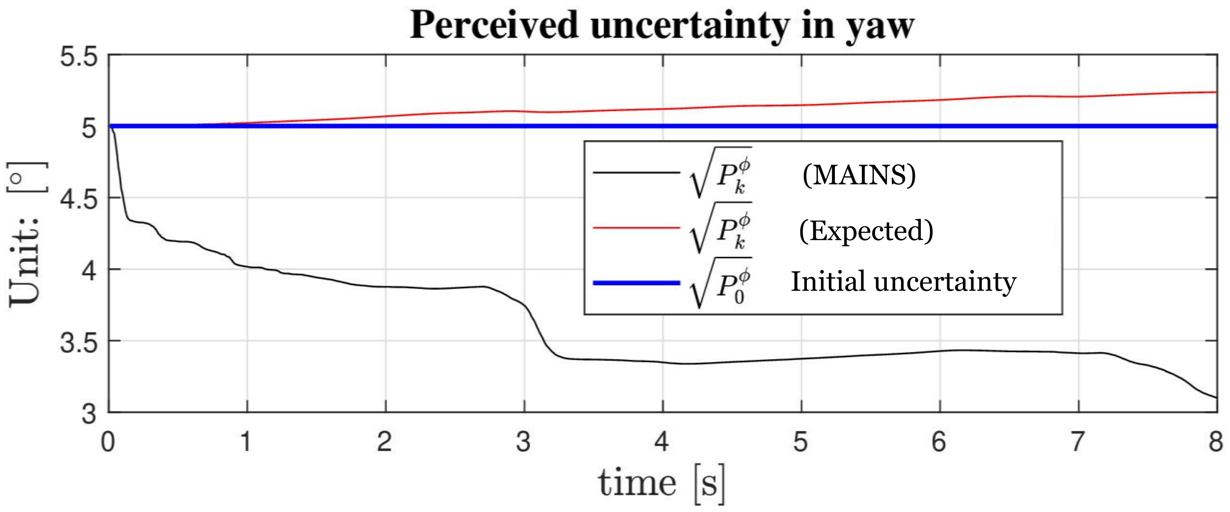

- The decreased perceived uncertainty in yaw is a strong indication that the estimate is inconsistent.
- The inconsistency is caused by false observability[1], resulting from linearization.

The inconsistency must be handled carefully!

[1] Huang, G.P., Mourikis, A.I. and Roumeliotis, S.I. "A first-estimates Jacobian EKF for improving SLAM consistency." Experimental Robotics: The Eleventh International Symposium. Springer Berlin Heidelberg, 2009.

Observability-Constrained Extend Kalman Filter (OC-EKF)[1]

Overview

$$x_{k+1} = f(x_k, u_k, w_k), \tag{1a}$$
$$y_k = h(x_k) + e_k. \tag{1b}$$

Step 1: Construct **local observability matrix** for nonlinear system (1).

Step 2: Find the **unobservable subspace** of the linearized system.

Step 3: Modify the Jacobian matrices used in a normal EKF.

[1] Hesch, J.A., Kottas, D.G., Bowman, S.L. and Roumeliotis, S.I., 2013.
Consistency analysis and improvement of vision-aided inertial navigation. *IEEE Transactions on Robotics*, *30*(1), pp.158-176.

Contribution

- Derive analytic expressions for unobservable subspace for the MAINS.
- Extend OC-EKF (in Step 3) so that the Jacobian matrices modifications are less in some situations.
- Evaluate the proposed method on simulated and real-world datasets.

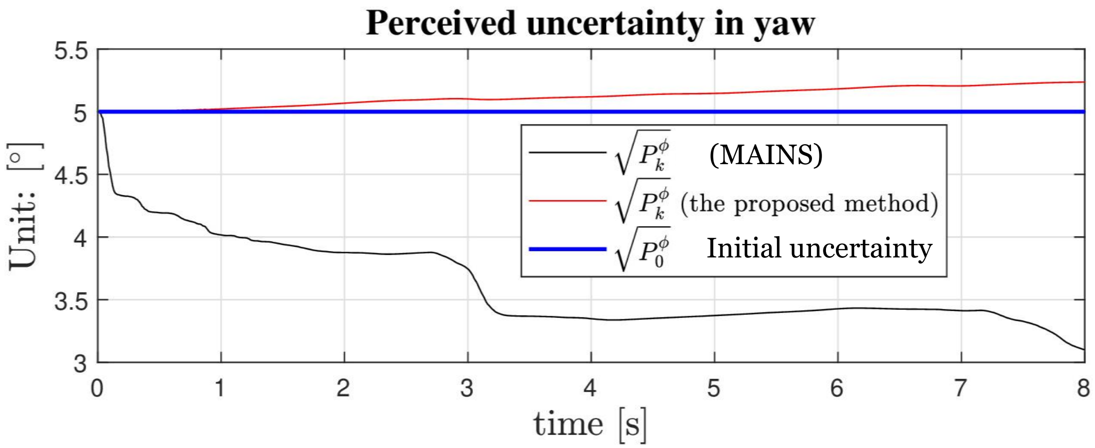

Application to the MAINS

Step 1: Construct local observability matrix

$$\bar{\mathcal{O}}_k \doteq \begin{bmatrix} \bar{H}_k \\ \bar{H}_{k+1}\bar{\Phi}(k+1,k) \\ \vdots \\ \bar{H}_{k+n_x-1}\bar{\Phi}(k+n_x-1,k) \end{bmatrix}. \tag{1a}$$

where

$$\bar{\Phi}(k+i,k) = \bar{F}_{k+i-1}\bar{F}_{k+i-2}\cdots\bar{F}_k, \tag{1b}$$

$$\bar{H}_k = \left.\frac{\partial h}{\partial x_k}\right|_{x_k=\bar{x}_k} \quad \text{and} \quad \bar{F}_k = \left.\frac{\partial f}{\partial x_k}\right|_{x_k=\bar{x}_k, u_k=\bar{u}_k, w_k=0}. \tag{1c}$$

$\bar{x}_{k:k+n_x-1}$: the nominal trajectory, where $\bar{x}_{k+1} = f(\bar{x}_k, \bar{u}_k, w_k = 0)$.

Application to the MAINS

Step 2: Find the unobservable subspace for the linearized system

$N(\cdot)$ is a function that outputs the basis vectors of $\bar{O}_k$'s nullspace.

$$N : \mathbb{R}^{n_x} \to \mathbb{R}^{n_x \times d}$$

Such that $\bar{\mathcal{O}}_k N(\bar{x}_k) = 0, \quad \mathcal{N}_k = \text{span}\{N(\bar{x}_k)\}$. Here $\mathcal{N}_k$ denotes the nullspace of $\bar{\mathcal{O}}_k$.

Application to the MAINS

Step 3 (Original): Modify the Jacobian matrices used in a normal EKF.

Let the unmodified Jacobians be

$$\hat{F}_k = \left.\frac{\partial f}{\partial x_k}\right|_{x_k=\hat{x}_{k|k},u_k=\hat{u}_k,w_k=0} \quad \text{and} \quad \hat{H}_k = \left.\frac{\partial h}{\partial x_k}\right|_{x_k=\hat{x}_{k|k-1}} \tag{1}$$

The modified Jacobians are obtained by solving the optimization problem as follows

$$\tilde{F}_k^* = \arg\min_{\tilde{F}_k} \|\tilde{F}_k - \hat{F}_k\|_{\mathcal{F}}^2 \qquad \tilde{H}_k^* = \arg\min_{\tilde{H}_k} \|\tilde{H}_k - \hat{H}_k\|_{\mathcal{F}}^2$$

$$\text{s.t.} \quad N(\hat{x}_{k+1|k}) = \tilde{F}_k N(\hat{x}_{k|k-1}), \qquad \text{s.t.} \quad \tilde{H}_k N(\hat{x}_{k|k-1}) = 0.$$

$\mathcal{F}$: Frobenius norm.

Application to the MAINS

Step 3 (Extension): Modify the Jacobian matrices used in a normal EKF.

Let the unmodified Jacobians be

$$\hat{F}_k = \frac{\partial f}{\partial x_k}\bigg|_{x_k=\hat{x}_{k|k},u_k=\hat{u}_k,w_k=0} \quad \text{and} \quad \hat{H}_k = \frac{\partial h}{\partial x_k}\bigg|_{x_k=\hat{x}_{k|k-1}} \tag{1}$$

The modified Jacobians are obtained by solving the optimization problem as follows

$$\tilde{F}_k^* = \arg\min_{\tilde{F}_k} \|\tilde{F}_k - \hat{F}_k\|_{\mathcal{F}}^2 \qquad \tilde{H}_k^* = \arg\min_{\tilde{H}_k} \|\tilde{H}_k - \hat{H}_k\|_{\mathcal{F}}^2$$

$$\text{s.t.} \quad N(\hat{x}_{k+1|k})\mathcal{E}_{k+1} = \tilde{F}_k N(\hat{x}_{k|k-1})\mathcal{E}_k, \qquad \text{s.t.} \quad \tilde{H}_k N(\hat{x}_{k|k-1})\mathcal{E}_k = 0.$$

Here $\mathcal{E}_{k+1}, \mathcal{E}_k$ are full rank square matrices.

Simulations and Experiment Results

Simulation Setup

Monte Carlo simulation

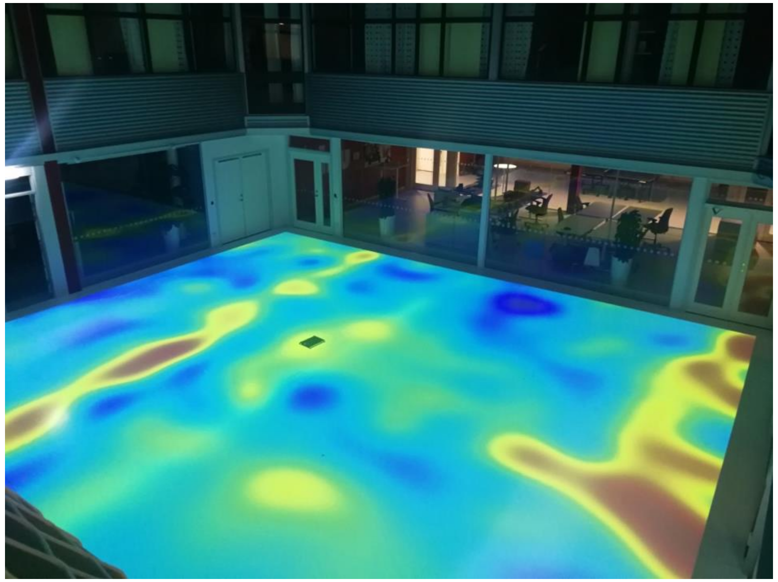

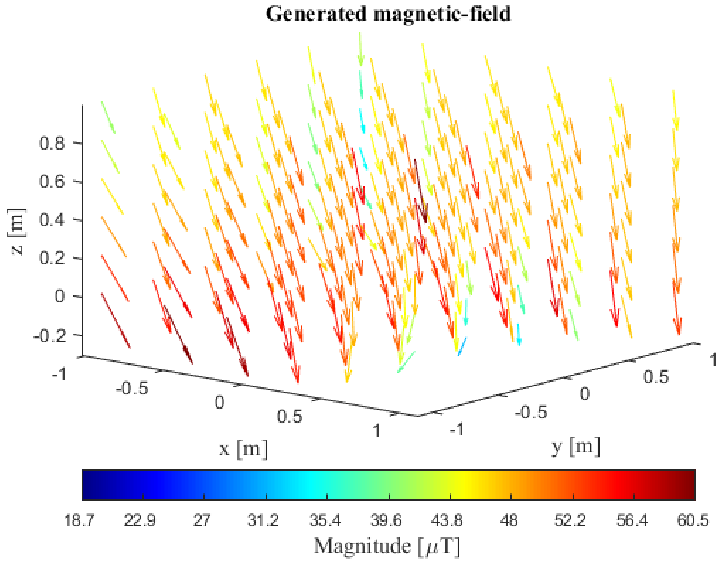

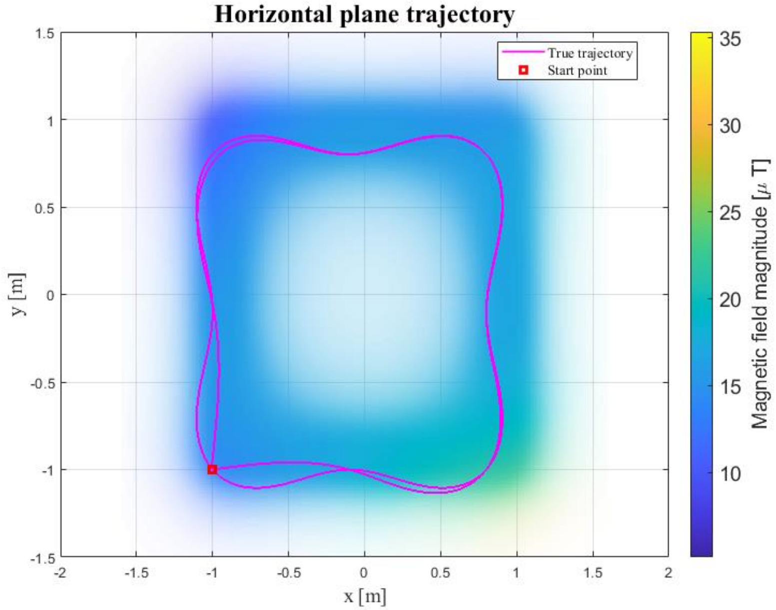

Simulation Results

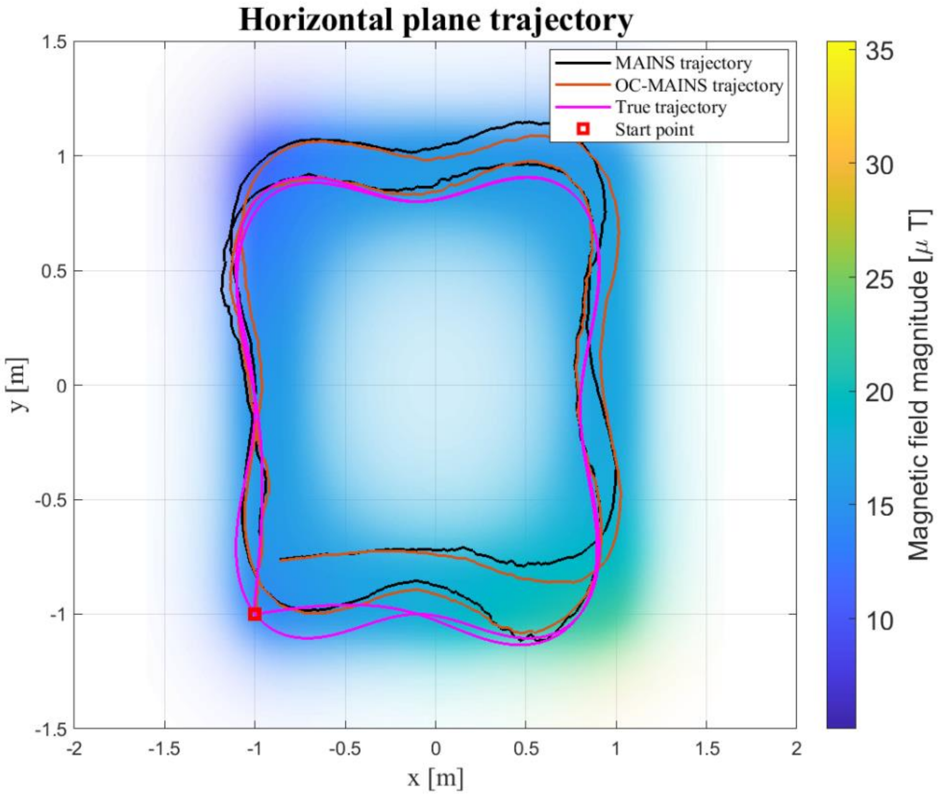

- Both trajectories end at almost same place.

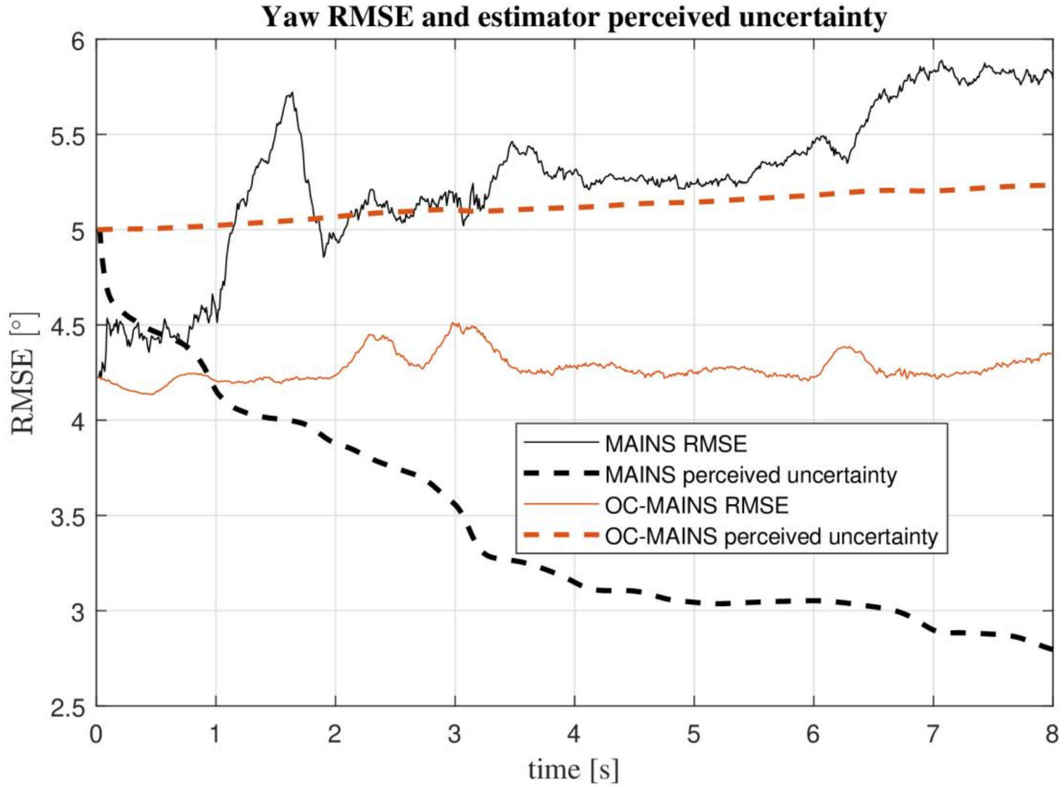

- More consistent uncertainty in yaw.
- Improved yaw accuracy.

Real-World Experiment Setup

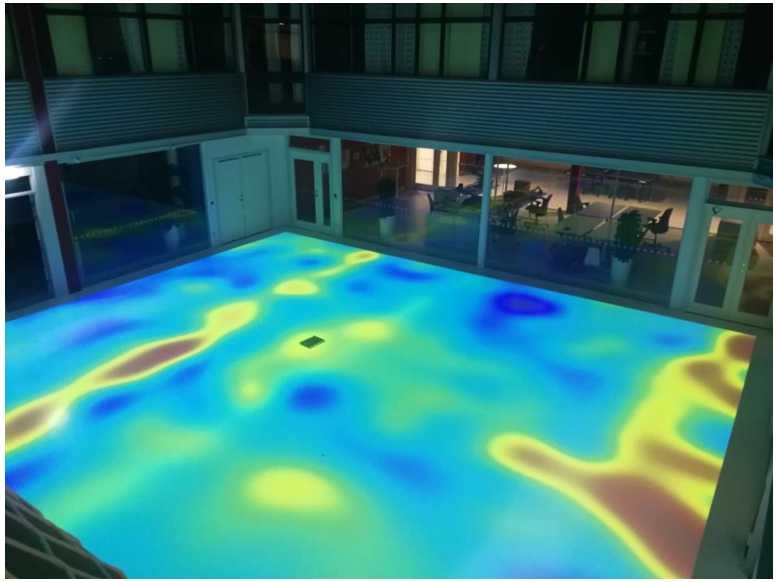

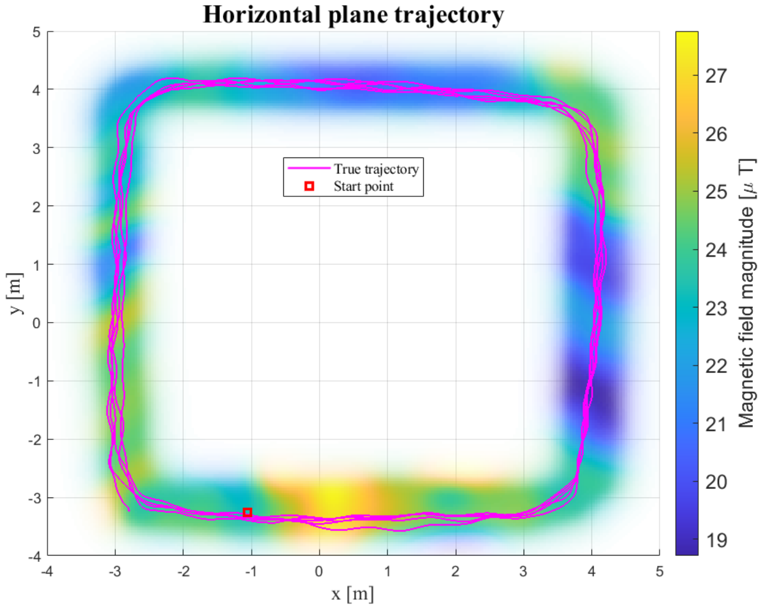

Real-World Experiment Results

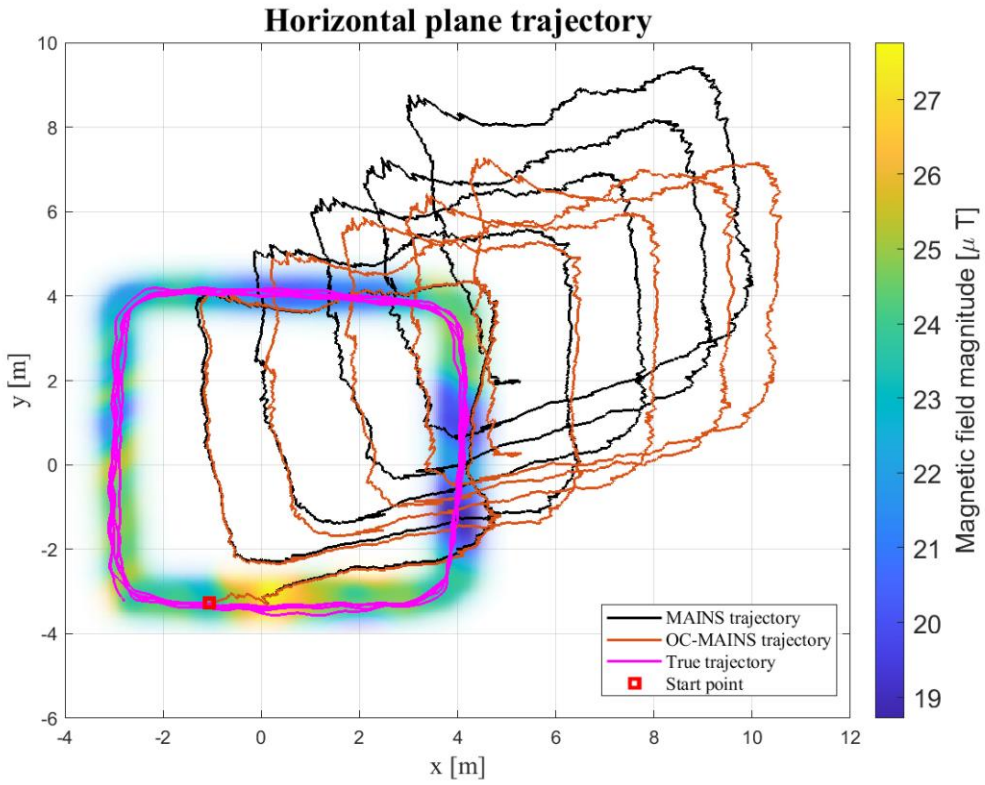

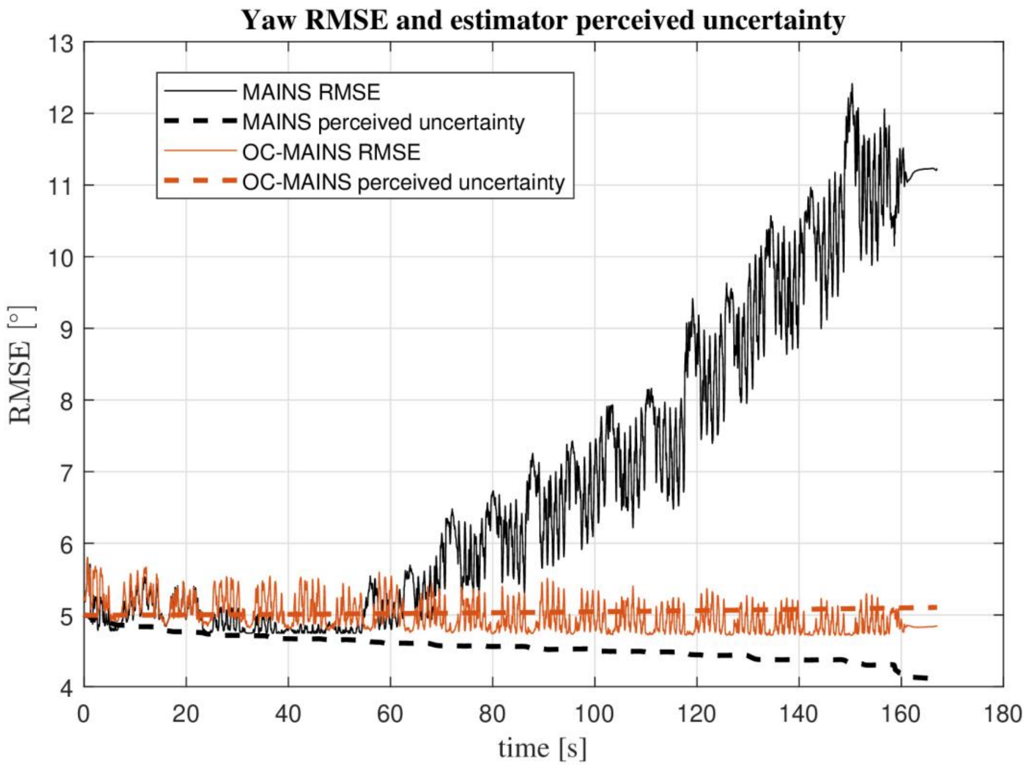

- The drift in the x and y directions could be due to IMU biases that have not been fully estimated.

- More consistent uncertainty in yaw.
- Improved yaw accuracy.

Conclusion

- The OC-EKF can be applied to the MAINS to improve consistency in **perceived uncertainty** in yaw.
- The RMSE of yaw in OC-MAINS is smaller.

Concluding Remarks

Summary

- An efficient and easy-to-use IMU-magnetometer calibration method
- A magnetic field-aided inertial navigation system
- An observability-constrained magnetic field-aided inertial navigation system

Published & Accepted Papers

A tightly-integrated magnetic-field aided inertial navigation system.

Chuan Huang, Gustaf Hendeby, and Isaac Skog.

In Proc. 2022 25th Int. Conf. on Information Fusion (FUSION), pages 1–8, Linköping, Sweden, July 2022.

MAINS: A magnetic-field-aided inertial navigation system for indoor positioning.

Chuan Huang, Gustaf Hendeby, Hassen Fourati, Christophe Prieur, and Isaac Skog. IEEE Sensors Journal, 24(9):15156–15166, 2024.

An observability-constrained magnetic field-aided inertial navigation system.

Chuan Huang, Gustaf Hendeby, and Isaac Skog.

arXiv preprint arXiv:2406.02161. (Accepted to IPIN 2024)

Thank you!

On Indoor Localization Using Magnetic Field-Aided Inertial Navigation Systems

chuan.huang@liu.se

LINKÖPING UNIVERSITY